

Supplement of Atmos. Chem. Phys., 19, 9125–9152, 2019
<https://doi.org/10.5194/acp-19-9125-2019-supplement>
© Author(s) 2019. This work is distributed under
the Creative Commons Attribution 4.0 License.



Supplement of

Biomass burning aerosol over the Amazon: analysis of aircraft, surface and satellite observations using a global aerosol model

Carly L. Reddington et al.

Correspondence to: Carly L. Reddington (c.l.s.reddington@leeds.ac.uk)

The copyright of individual parts of the supplement might differ from the CC BY 4.0 License.

S1. Calculation of aerosol water uptake for simulated aerosol optical depth

S1.1 Description of the online water uptake calculation

In GLOMAP, the water uptake for each soluble aerosol component is calculated online according to Zdanovskii-Stokes-Robinson (ZSR) theory, which estimates the liquid water content as a function of solute molarity (Stokes and Robinson, 1966). For POM in the soluble modes, we assigned an hygroscopicity consistent with a water uptake per mole at 65% of that of SO₄ (Mann et al., 2010). This is likely to be an upper estimate of aerosol hygroscopicity as discussed in Reddington et al. (2016). When using ZSR to calculate water uptake in GLOMAP, the model relative humidity (from ECMWF reanalyses) is restricted to between 10 and 90%. In the calculation of aerosol optical depth (AOD), we used the resulting hourly mean aerosol wet radii and refractive indices to calculate the hourly aerosol extinction.

S1.2 Description of the offline κ-Köhler water uptake calculation

To calculate the water uptake “offline” we used the κ-Köhler scheme, based upon the Köhler equation with a single parameter, κ, defining the water uptake for different chemical species (Petters and Kreidenweis, 2007). The species-dependent hygroscopicity parameter, κ, is defined through its effect upon the water activity of the solution as follows:

$$\frac{1}{a_w} = 1 + \kappa \frac{V_s}{V_w},$$

where V_s is the volume of the dry aerosol and V_w is the volume of water. For the SO₄ and sea spray components in the model we used the mean values of κ for ammonium sulphate and sodium chloride for subsaturated air masses (0.53 and 1.12, respectively) from Petters and Kreidenweis (2007). BC is considered entirely hydrophobic in this model when using this scheme. We assume a κ value for POM (0.1) based upon aerosol samples collected during the 2008 Amazonian Aerosol Characterization Experiment (AMAZE-08) (Gunthe et al., 2009).

Using Köhler theory and the above equation, the relationship between the relative humidity and the growth of the aerosol can be defined as follows (see Petters and Kreidenweis (2007) for derivation):

$$S(D) = \frac{D^3 - D_d^3}{D^3 - D_d^3(1 - \kappa)} \exp\left(\frac{4\sigma_{s/a}M_w}{RT\rho_w D}\right),$$

where S is the saturation ratio, D_d is the dry diameter, D is the wet diameter, κ is the hygroscopic parameter specific to the solute, $\sigma_{s/a}$ is the surface tension of the droplet, R is the universal gas constant, T is the temperature and M_w and ρ_w are the molecular mass and density of water, respectively. In the model this equation is solved iteratively by incrementing D until the saturation ratio is equal to the ambient relative humidity. The growth factor and volume of water can be determined from this and used to calculate the refractive index of the wetted aerosol.

S2. Instrument description and measurement uncertainties

S2.1 Aircraft measurements

Submicron non-refractory aerosol composition was measured by a compact Time of Flight Aerosol Mass Spectrometer (cToF-AMS; Aerodyne Research, USA). For operating principles see Canagaratna et al., (2007) and Drewnick et al., (2005); for operation on the BAe-146 aircraft

see Morgan et al., (2009); and for calibrations and post processing undertaken for this work see Allan et al., (2014). The combined measurement uncertainties are ~30% (Bahreini et al., 2009; Middlebrook et al., 2012).

Refractory Black Carbon (rBC) mass concentrations were measured by a Single Particle Soot Photometer (SP2; Droplet Measurement Technologies, USA). For operating principles see Baumgardner et al., (2004) and Stephens et al., (2003); for operation on the BAe-146 aircraft see McMeeking et al., (2010); and for calibrations and processing undertaken for this work see Allan et al., (2014). Reported mass loadings have a measurement uncertainty of ~30% (Schwarz et al., 2008; Shiraiwa et al., 2008).

Aerosol number-size distributions were measured across the 20 nm to 20 μm diameter range. A Scanning Mobility Particle Sizer (SMPS, TSI-Inc; Wang and Flagan, (1990)) steps through voltages equivalent to electrical mobility diameters between 20 and 350 nm, measuring aerosol number at each with a TSI Inc. Water-based Condensation Particle Counter (WCPC, Model 3786-LP; Herring et al., 2005). As the SMPS voltage scan takes ~1 minute, distributions are only valid for periods without rapid environmental change and hence unavailable for vertical profile analysis. A GRIMM model 1.108 Optical Particle Counter (OPC; Heim et al., (2008)), detects and discretises scattered light into time bins related to aerosol diameters between ~0.3 and 20 μm .

Aerosols are sampled into the BAe-146 aircraft through a Rosemount inlet. Whilst line losses are possible at larger sizes, the transmission of submicron particles is considered adequate (Trembath, 2013).

S2.2 Ground measurements

The aethalometer has been corrected for filter loading and multiple scattering according to Arnott et al., (2005) and Schmid et al., (2006) using aerosol scattering measurements from a nephelometer. The uncertainty of the instrument under those conditions (95% confidence level) has been estimated at 20% (Schmid et al., 2006).

The Aerosol Chemical Speciation Monitor (ACSM) has been calibrated using NH_4NO_3 monodispersed aerosols following the procedure described by Ng et al., (2011). The associated uncertainty for organics, which is the largest contributor to NR-PM₁ (non-refractory particulate matter with aerodynamic diameter $\leq 1 \mu\text{m}$) during the SAMBBA field campaign, has been estimated at 15 %, whereas other minor species have estimated uncertainties ranging from 9 % to 36 % (Crenn et al., 2015).

Both instruments have shown excellent agreement (R^2 : 0.90, slope 0.99) with integrated aerosol volume measured using an SMPS (Brito et al., 2014), providing confidence that the operation and calibration of the instruments falls well within the conditions described in the references aforementioned.

S2.3 Aerosol optical depth retrievals

Bias and uncertainty estimates for near-real-time AERONET AOD are computed by using the difference of the pre-field calibration AOD minus the interpolated calibration AOD (Giles et al., 2019). For AERONET version 3 data, the field instrument AOD 1σ uncertainty is estimated to be from 0.01 to 0.02 with the maximum representing the uncertainty only in the UV channels (340 and 380 nm), and the bias is estimated to be up to +0.02 (Giles et al., 2019). For MODIS Collection 5 AOD, the reported 1σ uncertainty is ± 0.05 +15% for the overland cases (Levy et al., 2010).

Supplementary figures

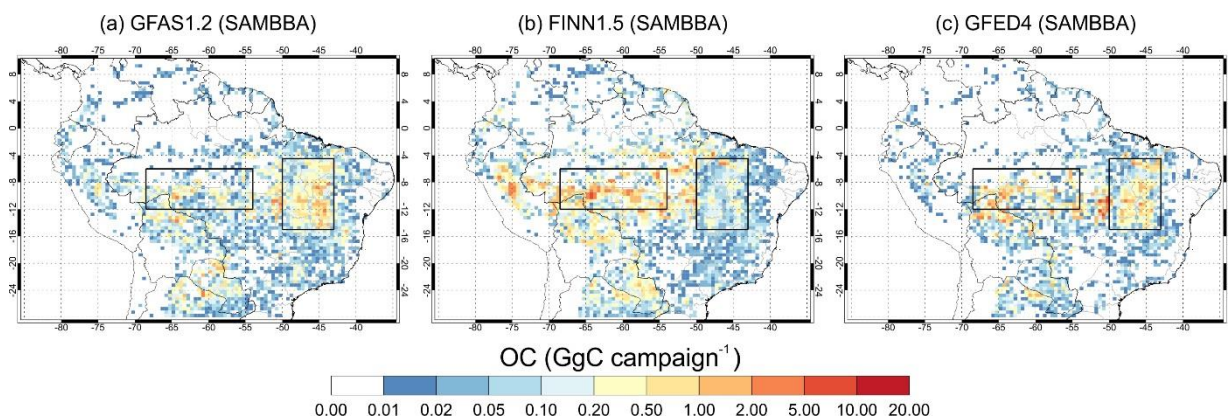


Figure S1. Estimated total organic carbon (OC) aerosol emissions from fire shown for the SAMBBA field campaign (13 September to 3 October 2012). Emissions are shown for **(a)** GFAS version 1.2, **(b)** FINN version 1.5 and **(c)** GFED version 4.1s. The eastern (43-50°W, 4.5-15°S) and western (54-68.5°W, 6-12°S) domains are shown with black boxes. The GFAS, FINN and GFED OC emissions were re-gridded onto a common grid of 0.5°x0.5° resolution for comparison.

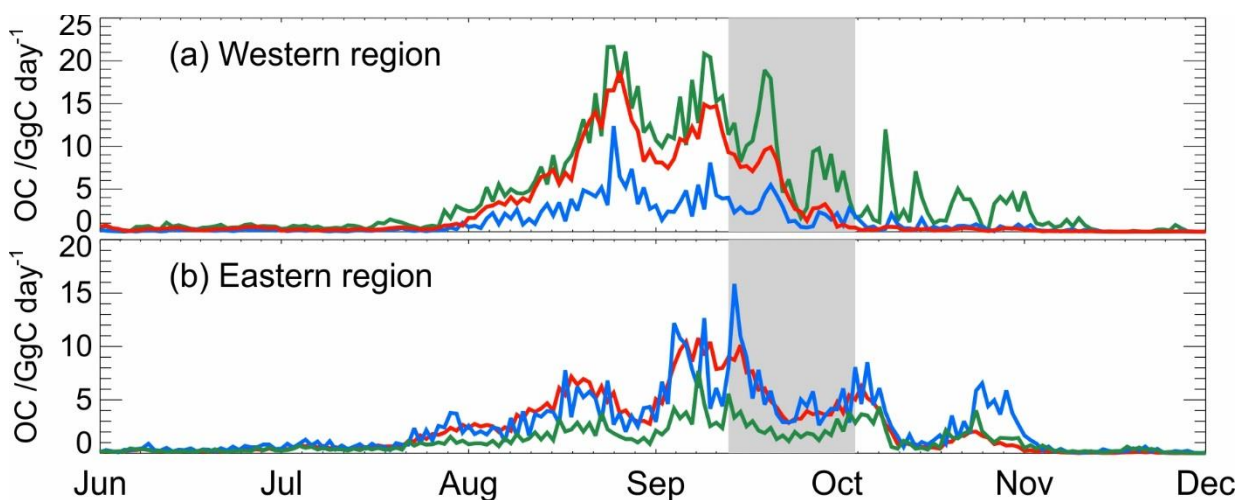


Figure S2. Total daily organic carbon (OC) aerosol emissions from fire for June – November 2012 over **(a)** the western Amazon (54-68.5°W, 6-12°S) and **(b)** the eastern Amazon (43-50°W, 4.5-15°S). Emissions are shown for GFAS version 1.2 (blue), FINN version 1.5 (green) and GFED version 4.1s (red). The SAMBBA campaign period (13 September – 3 October 2012) is shown in grey.

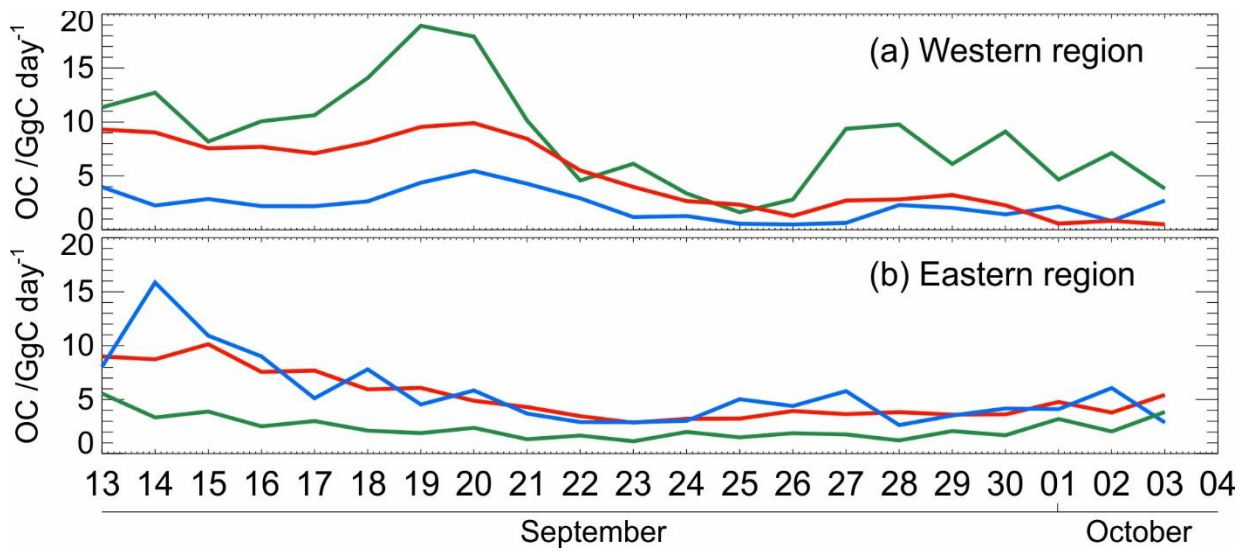


Figure S3. Total daily organic carbon (OC) aerosol emissions from fire for the SAMBBA campaign (13 September – 3 October 2012) over **(a)** the western Amazon (54-68.5°W, 6-12°S) and **(b)** the eastern Amazon (43-50°W, 4.5-15°S). Emissions are shown for GFAS version 1.2 (blue), FINN version 1.5 (green) and GFED version 4.1s (red).

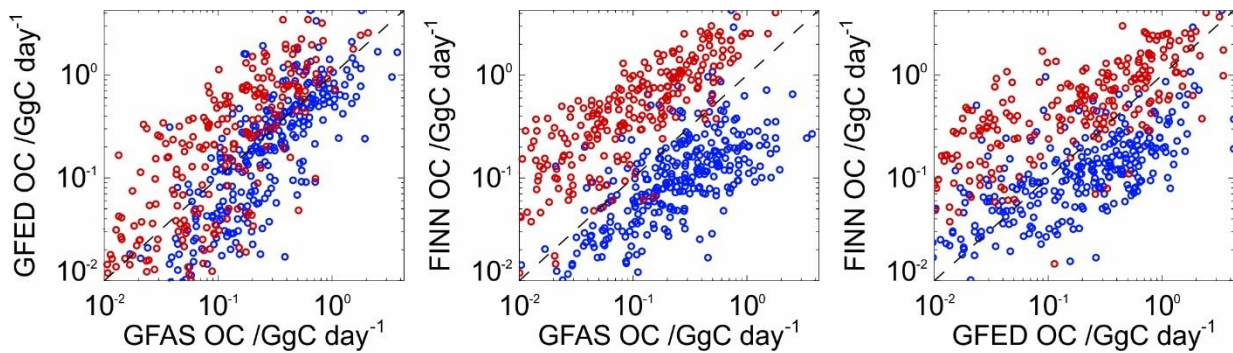


Figure S4. Total daily organic carbon (OC) aerosol emissions from fire in every 0.5°x0.5° grid cell the western Amazon (54-68.5°W, 6-12°S) (red) and the eastern Amazon (43-50°W, 4.5-15°S) (blue), during the SAMBBA campaign (13 September – 3 October 2012). Emissions are shown for GFAS version 1.2, FINN version 1.5 and GFED version 4.1s.

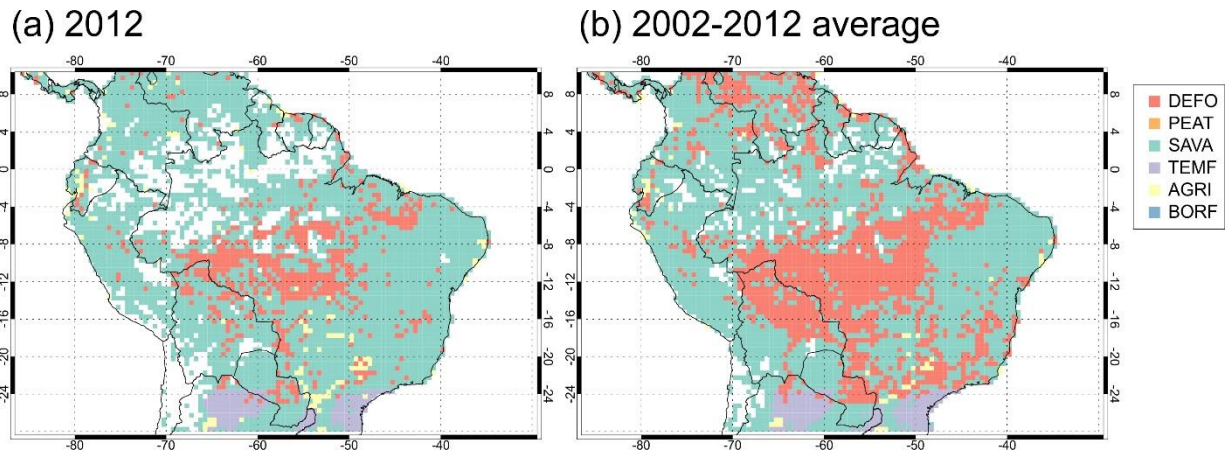


Figure S5. Spatial distribution of the dominant fire types for fire emissions of OC in the Amazon region for **(a)** 2012 and **(b)** 2002-2012. Data is from GFED4 (van der Werf et al., 2010; 2017) re-gridded to $0.5^\circ \times 0.5^\circ$ resolution to be consistent with Fig. 1. Fires are characterised into six types: deforestation and degradation fires (DEFO); peatland fires (PEAT); savanna, grassland, and shrubland fires (SAVA); temperate forest fires (TEMF); agricultural waste burning (AGRI); and boreal forest fires (BORF). The dominant fire type was derived by calculating the maximum GFED4 OC emissions flux for each fire type in each $0.5^\circ \times 0.5^\circ$ grid cell over the periods 2002-2012 and 2012.

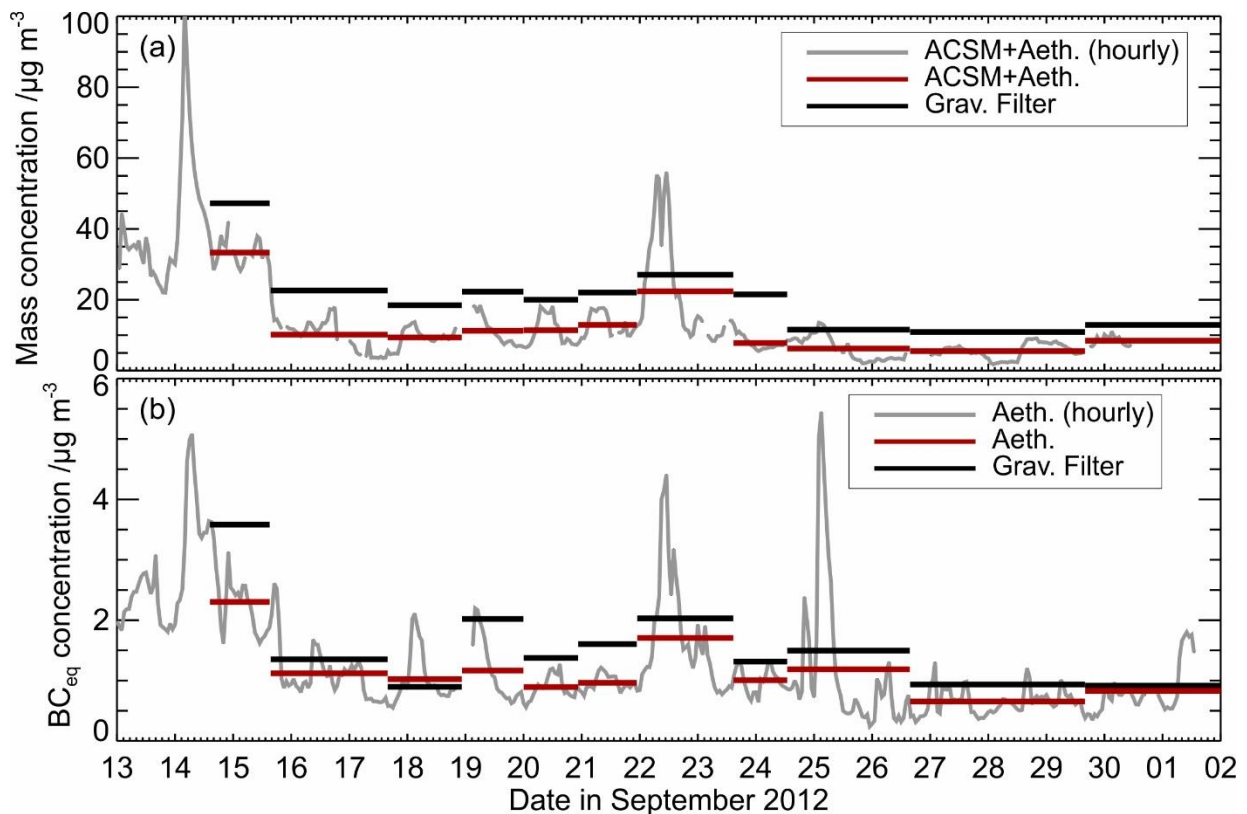


Figure S6. Time series of aerosol mass concentration measurements at Porto Velho ground station during the SAMBBA campaign. **(a)** Total aerosol mass concentration measured using gravimetric filter analysis (“Grav. Filter”; for aerosol $< 2.5 \mu\text{m}$ in diameter) and calculated as mass measured by the ACSM plus equivalent black carbon (BC_{eq}) measured by the aethelomter (“ACSM+Aeth.”; for aerosol in the 75 - 650 nm diameter range). **(b)** BC_{eq} measured using gravimetric filter analysis (“Grav. Filter”; for aerosol $< 2.5 \mu\text{m}$ in diameter) and the aethelomter (“Aeth.”). The ACSM and aethelomter hourly data were averaged over the measurement duration of the gravimetric filter samples.

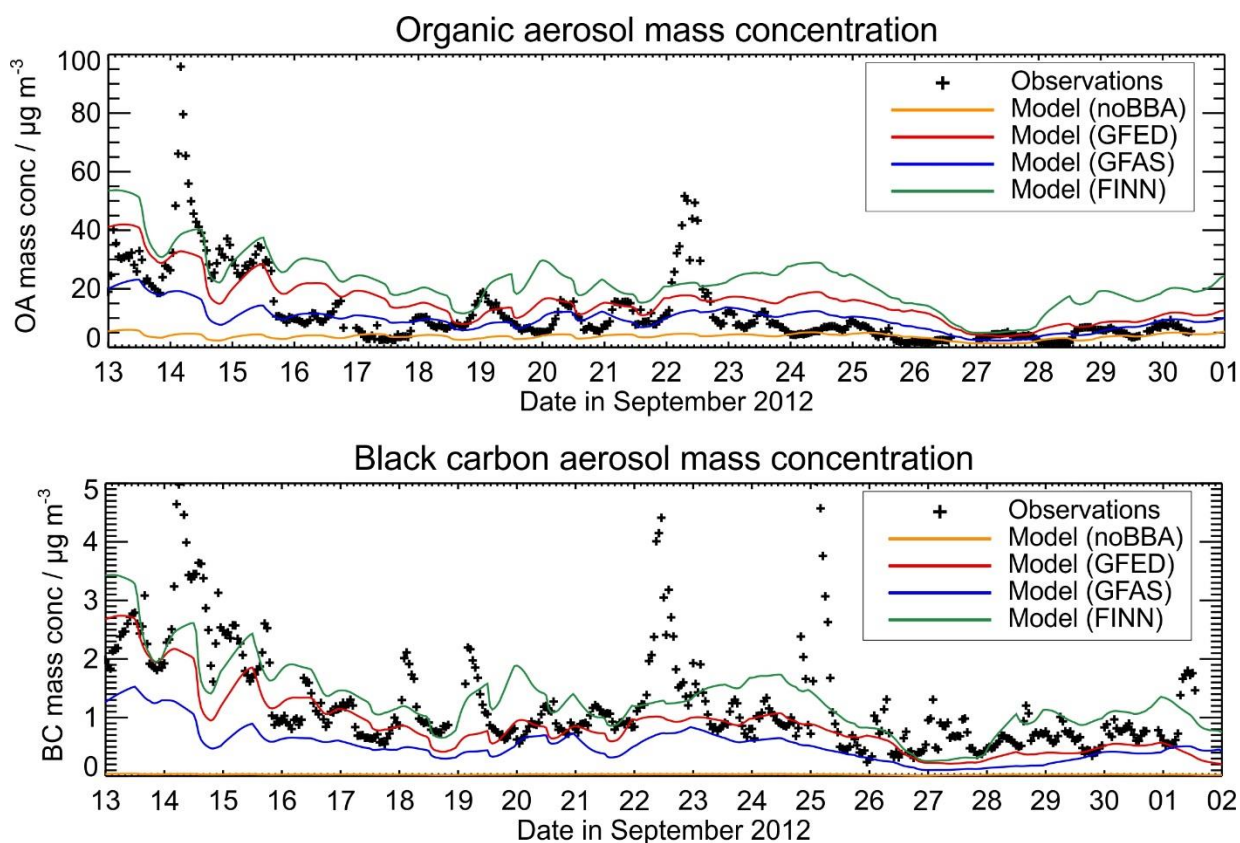


Figure S7. Time series of hourly-mean observed (black) and simulated (colour) organic aerosol (OA; top panel) and black carbon (BC; bottom panel) mass at Porto Velho ground station during the SAMBBA campaign. OA mass concentration was measured using the ACSM instrument; BC mass concentration was measured with the aethelometer. Simulated OA and BC mass concentrations are shown for the model with FINN1.5 (green), GFAS1.2 (blue), GFED4 (red) emissions and with no biomass burning emissions (noBBA; orange).

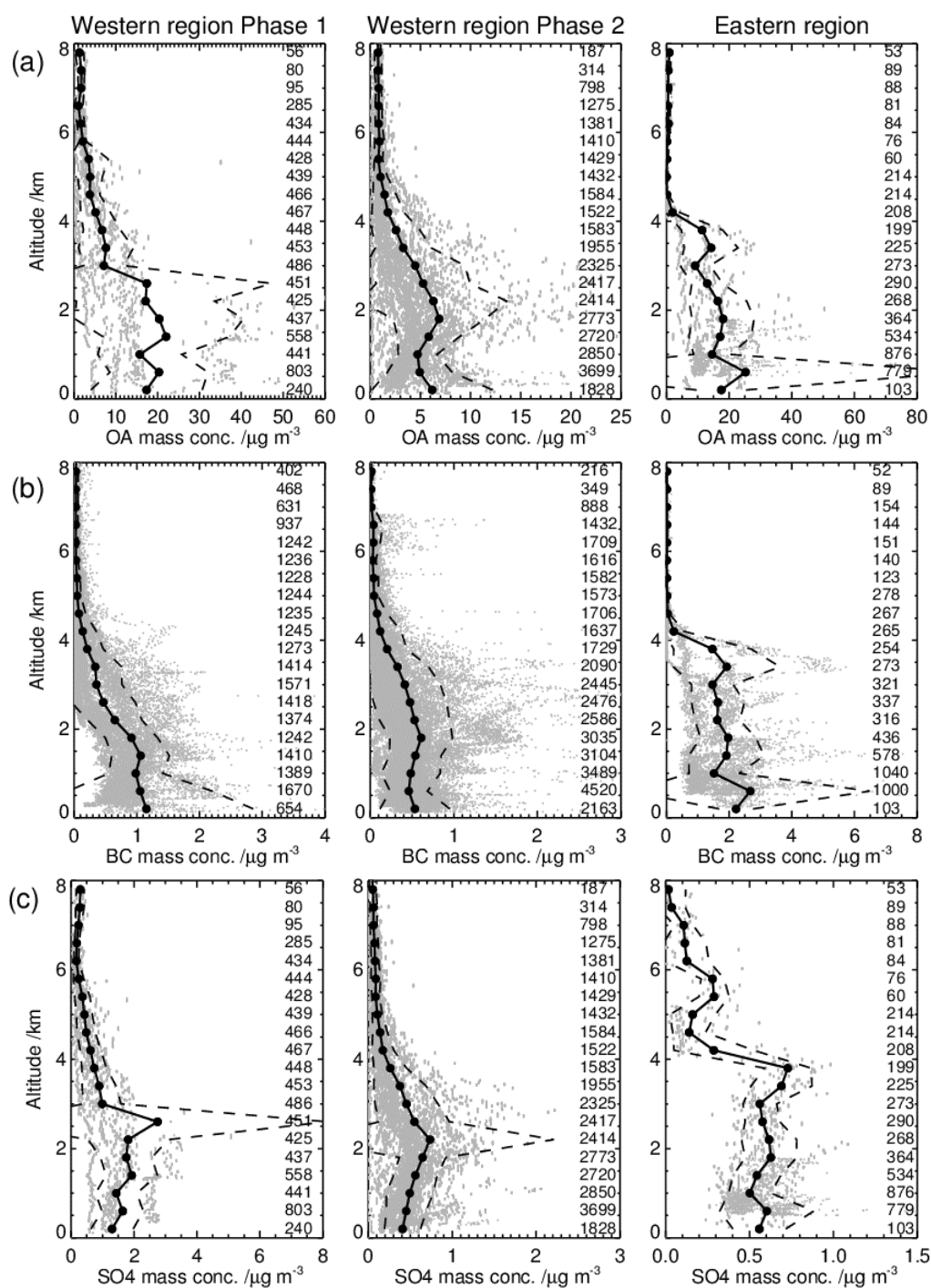


Figure S8. Mean observed vertical profiles of (a) organic aerosol (OA), (b) black carbon (BC) and (c) sulfate (SO₄) during the SAMBBA aircraft campaign, sectioned into 400 m altitude bins. The numbers on the right hand side give the number of valid observations (from either the AMS or SP2 instruments) per altitude bin. Black data points show campaign-mean values; dashed black lines show the standard deviation of the observed means; grey data points show all valid observed values. The observations are split into western and eastern regions of the Amazon (Fig. 2 and Fig. S1) and by time (Phase 1: 13/09/2012 – 22/09/2012, Phase 2: 23/09/2012 - 03/10/2012) for the western region.

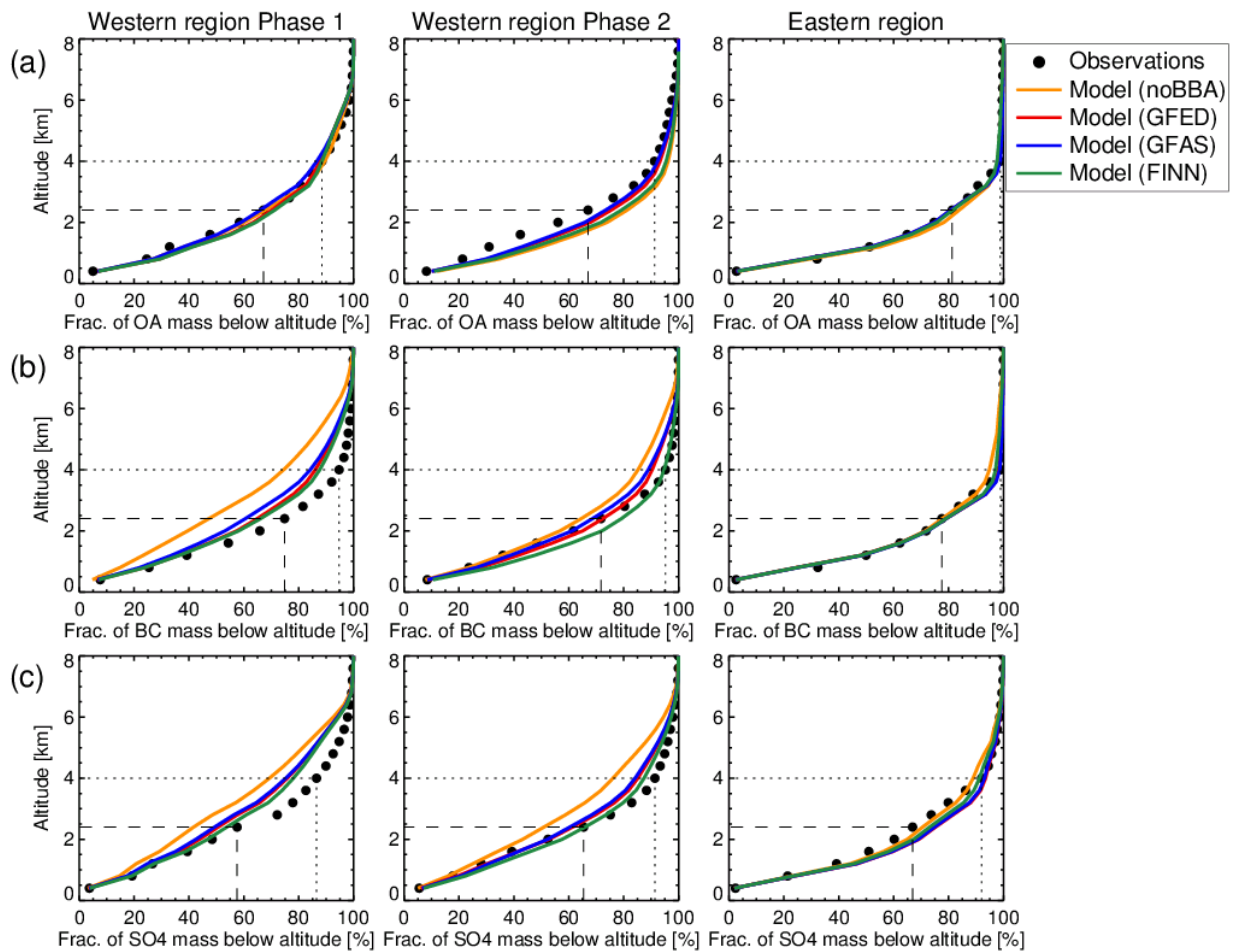


Figure S9. Mean vertical profiles of observed and simulated fraction of aerosol mass column for **(a)** organic aerosol (OA); **(b)** black carbon (BC); and **(c)** sulfate (SO₄) during the SAMBBA aircraft campaign, sectioned into 400 m altitude bins. Observations are shown by the black data points; simulated concentrations are shown for the model with FINN1.5 (green), GFAS1.2 (blue), GFED4 (red) emissions and with no biomass burning emissions (orange). The simulated data (linearly interpolated to the flight track of the aircraft) and the observations are split into western and eastern regions of the Amazon (Fig. 2 and Fig. S1) and by time (Phase 1: 13/09/2012 – 22/09/2012, Phase 2: 23/09/2012 - 03/10/2012) for the western region. The dashed and dotted lines indicate the fraction of observed aerosol mass below 2.4 km and 4 km altitude, respectively.

ECMWF Boundary Layer Height September 2012 Mean

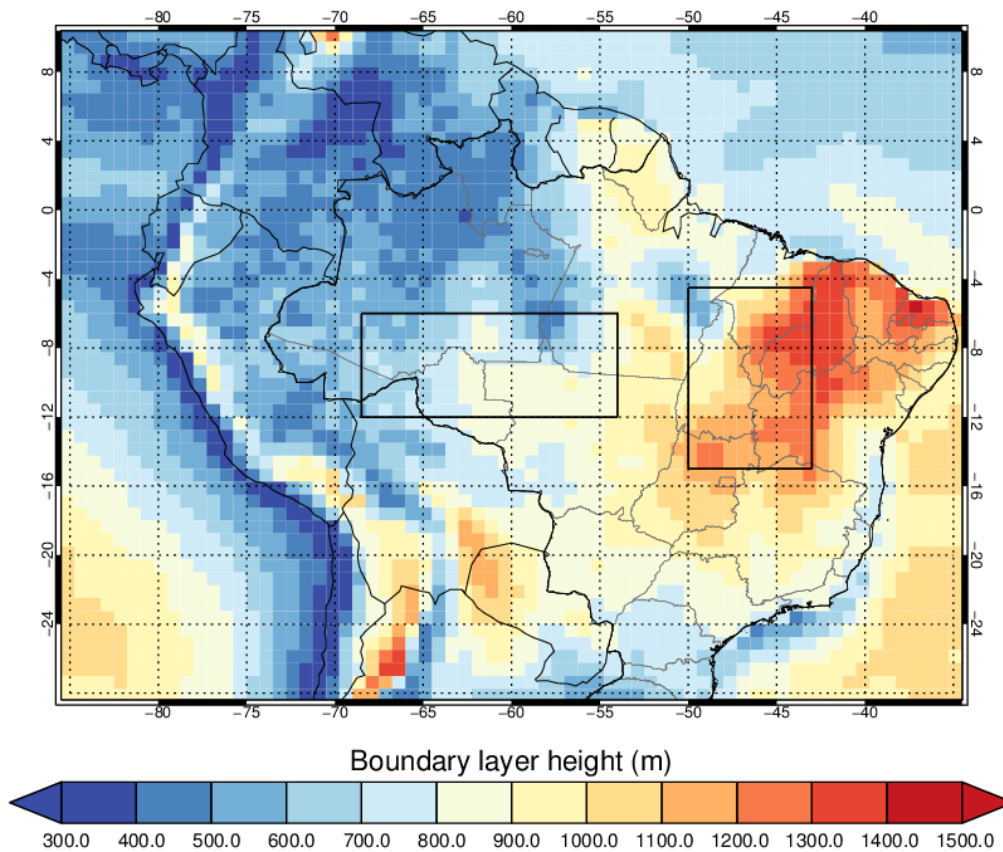


Figure S10. Map of the September 2012 mean boundary layer height over northern South America. Data is from the European Centre for Medium-Range Weather Forecasting (ECMWF) ERA-Interim reanalysis dataset (<https://www.ecmwf.int/en/forecasts/datasets/reanalysis-datasets/era-interim>). The September 2012 mean boundary layer height was calculated from daily means; data is available here: <https://apps.ecmwf.int/datasets/data/interim-full-moda/levtype=sfc/>. The eastern (43-50°W, 4.5-15°S) and western (54-68°W, 6.5-12°S) domains are shown with black boxes.

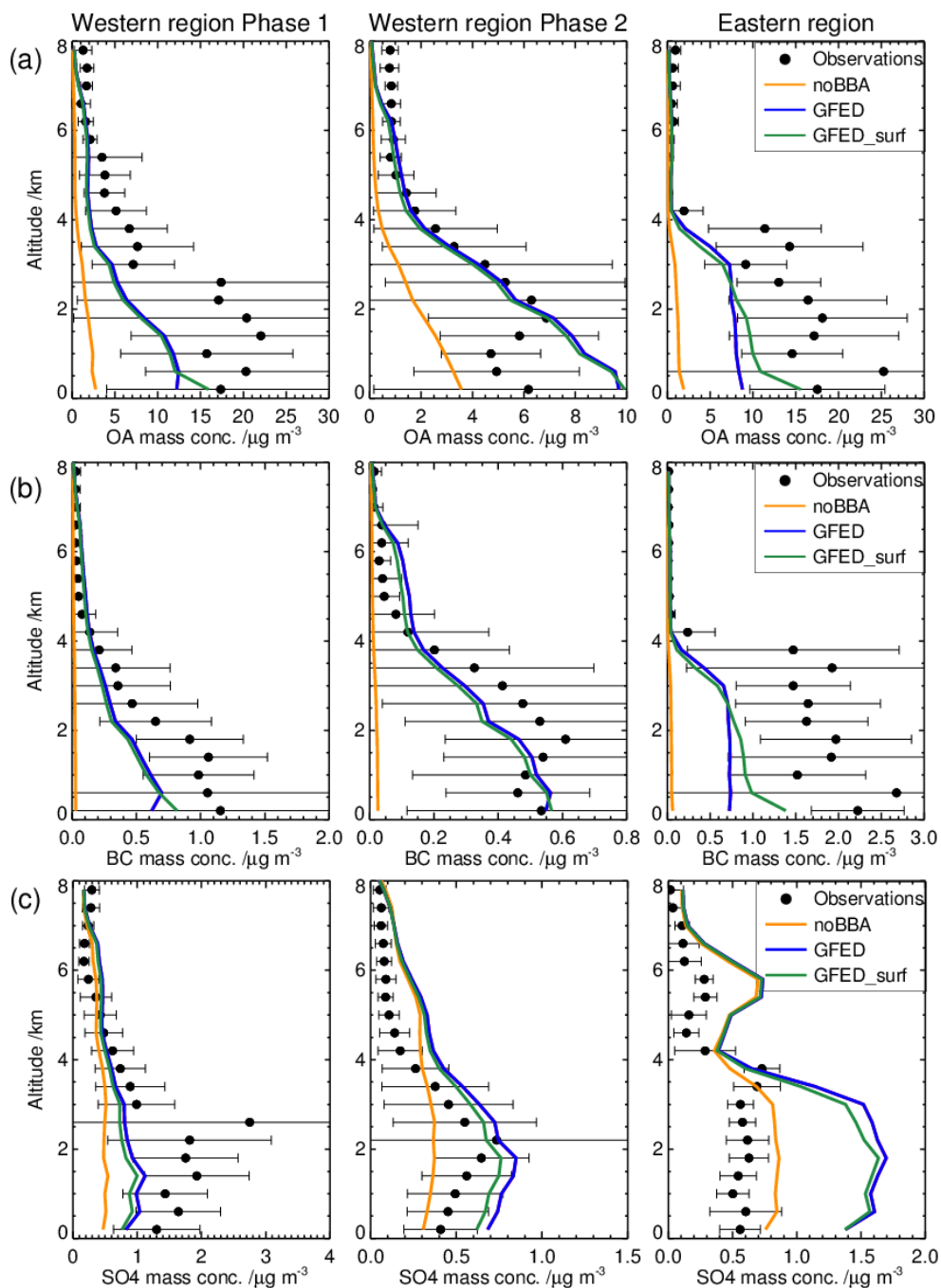


Figure S11. Mean observed and simulated vertical profiles of (a) organic aerosol (OA), (b) black carbon (BC) and (c) sulfate (SO₄) during the SAMBBA aircraft campaign, sectioned into 400 m altitude bins. Observations are shown by the black data points; simulated concentrations are shown for the model with no biomass burning emissions (noBBA; orange); with GFED4 emissions using AEROCOM-recommended injection heights (GFED; blue); and with GFED4 emissions injected into the surface layer of the model (GFED_surf; green). The simulated data (linearly interpolated to the flight track of the aircraft) and the observations are split into western and eastern regions of the Amazon (Fig. 2) and by time (Phase 1: 13/09/2012 – 22/09/2012, Phase 2: 23/09/2012 - 03/10/2012) for the western region. Error bars show the standard deviation of the observed mean. Concentrations are reported at standard temperature and pressure (STP) conditions (at 273.15 K and 1013.25 hPa).

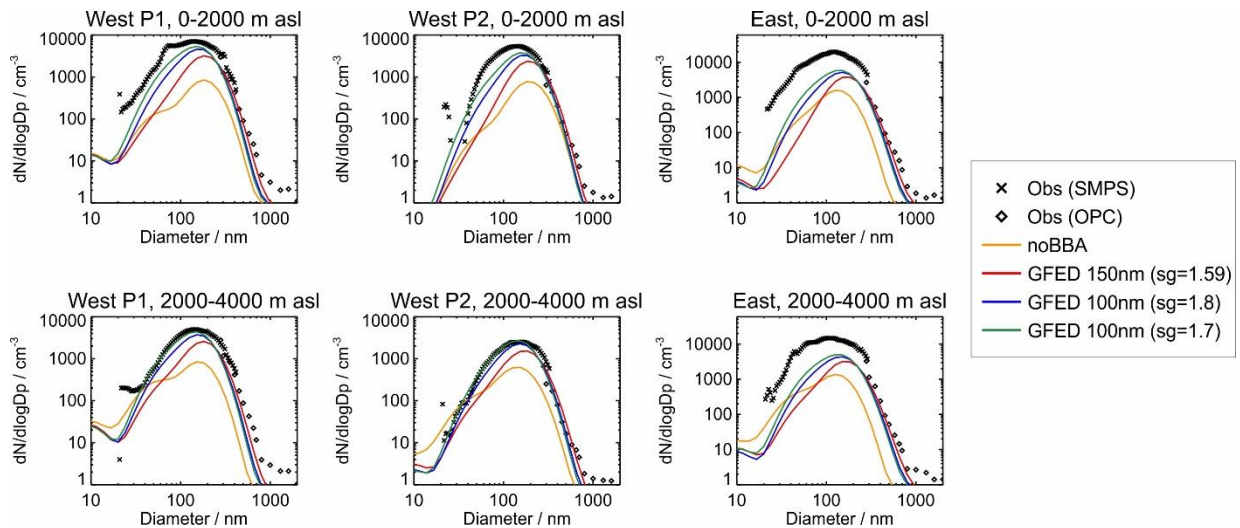


Figure S12. Mean observed (black) and simulated (colour) aerosol number size distributions during the SAMBBA aircraft campaign for two altitude bands: between the surface and 2 km (top panel) and between 2 and 4 km asl (bottom panel). The observed number size distribution was measured with Scanning Mobility Particle Sizer (SMPS; black crosses) and a Grimm optical particle counter (OPC; black diamonds). The simulated data (linearly interpolated to the flight track of the aircraft) and the observations are split into western and eastern regions of the Amazon (Fig. 2) and by time (P1: 13/09/2012 – 22/09/2012, P2: 23/09/2012 - 03/10/2012) for the western region. Simulated concentrations are shown for the model without biomass burning emissions (noBBA; orange line) and with GFED4 emissions assuming three different emission size distributions for primary biomass burning carbonaceous aerosol: 1) count median diameter (CMD) = 150 nm, modal width (sigma (sg)) = 1.59 (red line); 2) CMD = 100 nm, sg = 1.8 (blue line); and 3) CMD = 100 nm, sg = 1.7 (green line).

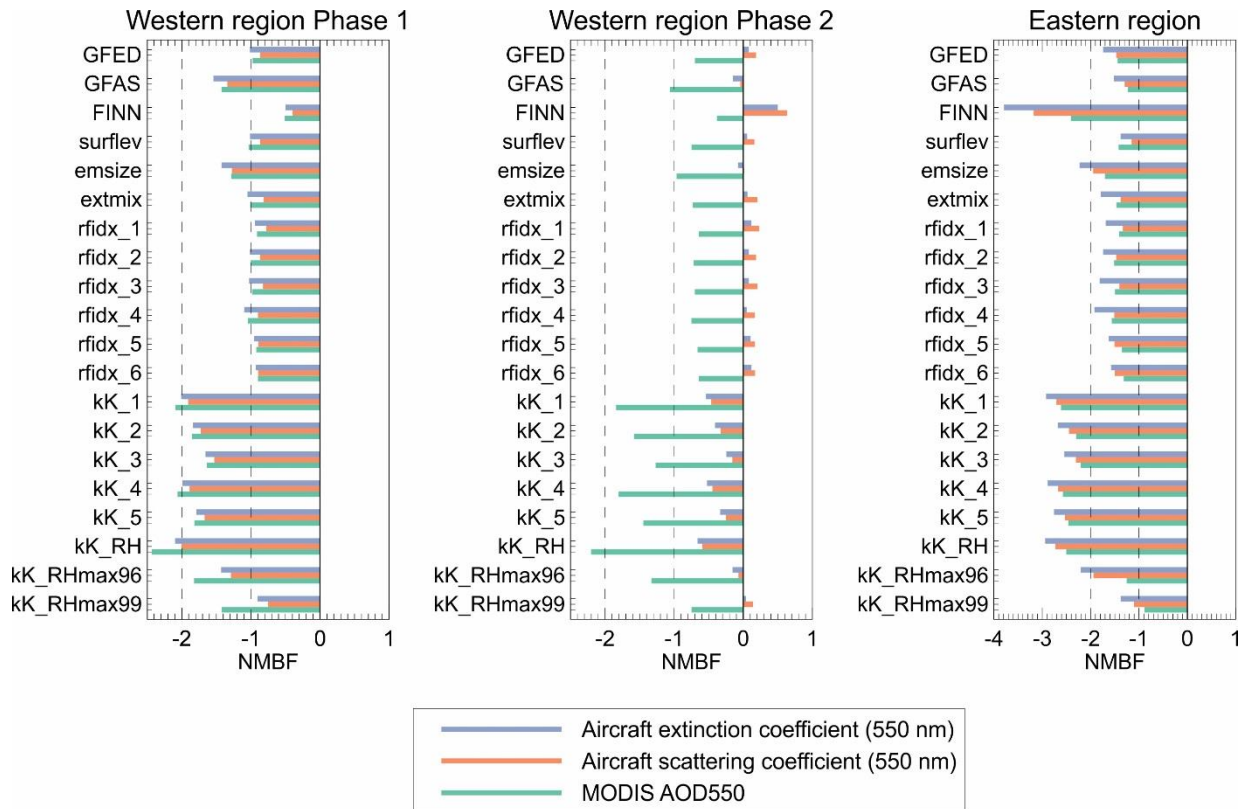


Figure S13. Summary of the normalised mean bias factor (NMBF) of simulated versus measured optical properties for the sensitivity simulations described in Table 3. Simulation names listed in the figure correspond to those listed in Table 3. NMBFs are calculated between simulated and satellite-retrieved (MODIS) AOD550; and between simulated and aircraft-measured aerosol scattering and extinction coefficients at 550 nm. Comparisons shown are for the SAMBBA campaign period (13 September – 3 October 2012) over the western Amazon (54-68.5°W, 6-12°S) during Phase 1 (left panel); the western Amazon during Phase 2 (middle panel); and the eastern Amazon (43-50°W, 4.5-15°S; right panel). For the comparison between simulations “κK_RH”, “κK_RHmax96” and “κK_RHmax99” (18, 19 and 20 in Table 3) and MODIS AOD550; data points from simulation “κK_1” (simulation 13 in Table 3) are used on days with no available aircraft measurements of RH. The dashed lines indicate NMBFs of -1 and -2 (equivalent to a factor 2 and a factor 3 model underestimation, respectively).

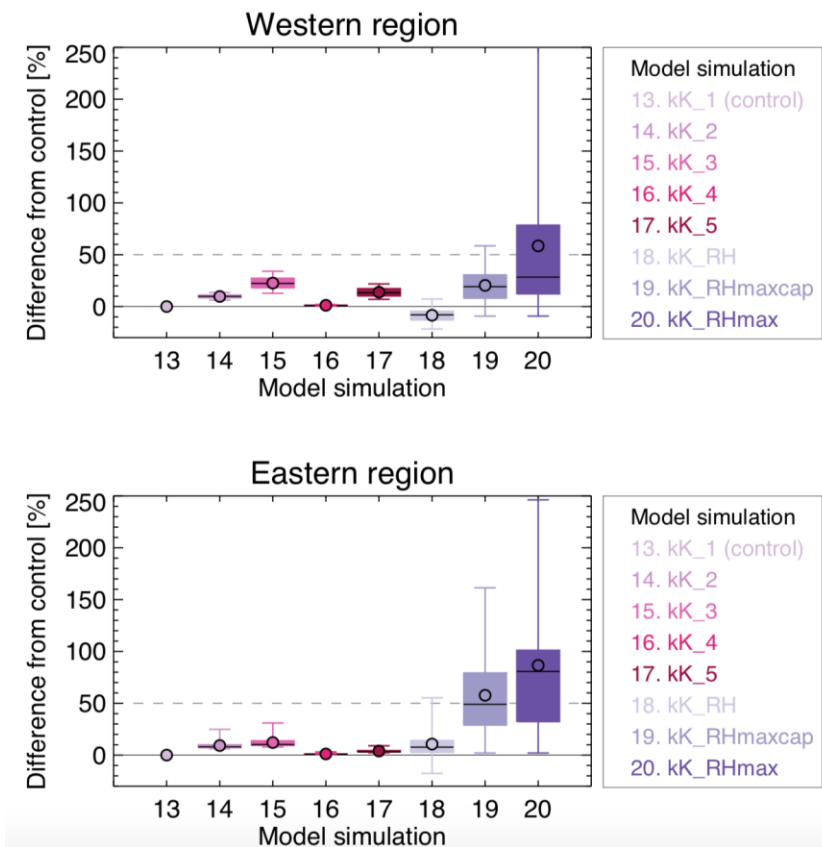


Figure S14. Box and whisker plot summarising the percentage difference between simulated hourly mean AOD550 from the control simulation (GFED emissions with κ -Köhler water uptake scheme) and sensitivity simulations 14 to 20 listed in Table 3. Simulation names and numbers in the figure correspond to those listed in Table 3. Simulations are compared during the SAMBBA campaign period (13 September – 3 October 2012) for the western region (54-68.5°W, 6-12°S; top panel) and the eastern region (43-50°W, 4.5-15°S; bottom panel) separately. Simulations 18, 19 and 20 are compared to the control simulation only on days with available aircraft measurements of RH. Circles show the mean values; whiskers show the minimum and maximum values; boxes show the 25th and 75th percentiles; and horizontal lines show the median values.

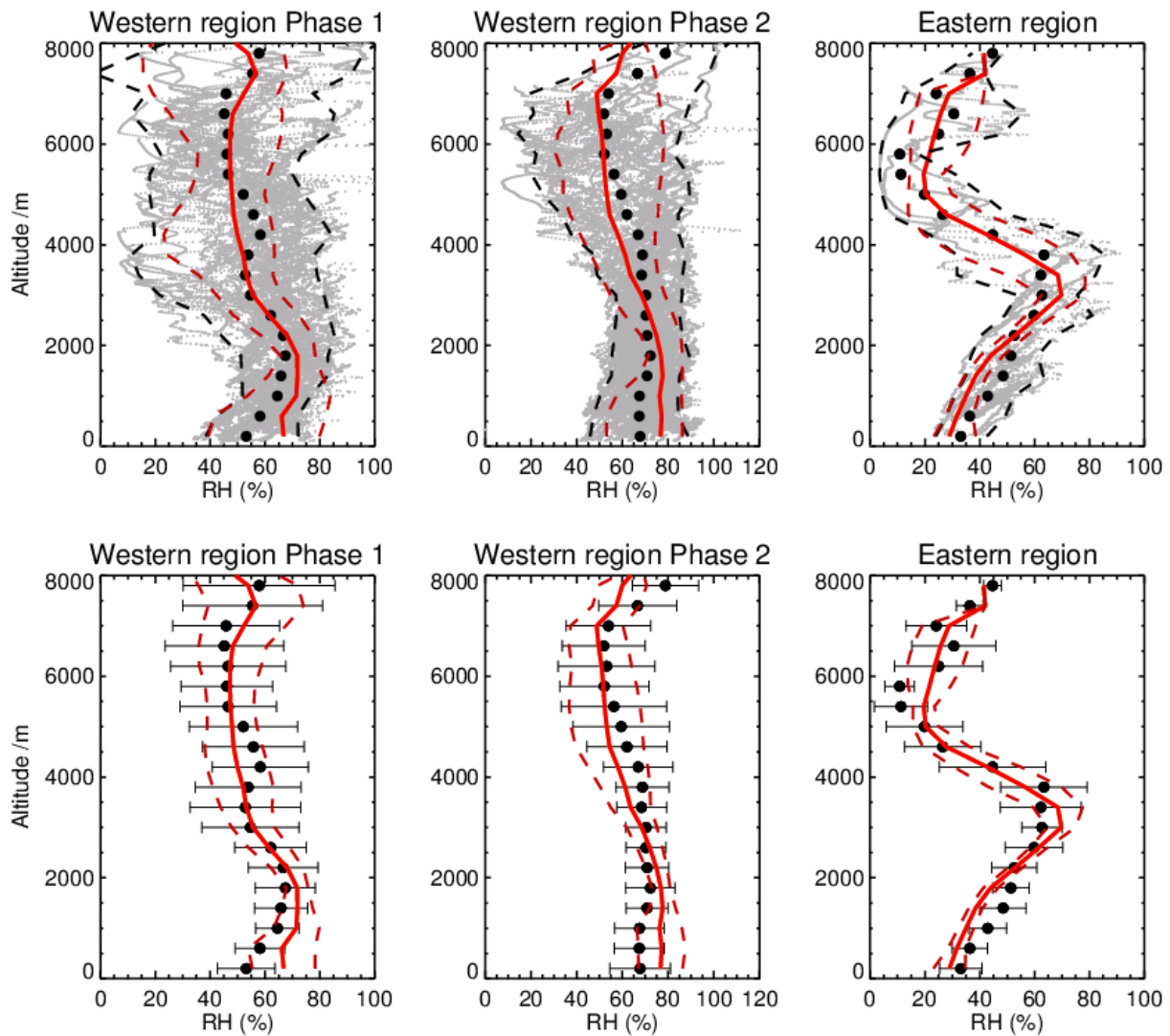


Figure S15. Mean observed (black) and simulated (red) vertical profiles of relative humidity (RH) during the SAMBBA aircraft campaign, sectioned into 400 m altitude bins. Upper panel: observed RH values are shown by the grey data points; campaign-mean observed RH values are shown by the black circles; campaign-mean GLOMAP RH values are shown by the red line; the observed simulated 5th and 95th percentiles are shown by the dashed lines. Bottom panel: campaign-mean observed and GLOMAP RH values are shown by the black circles and red line, respectively; the observed and GLOMAP standard deviations are shown by the black error bars and red dashed line, respectively. GLOMAP RH fields are from six-hourly ECMWF ERA-Interim reanalysis data, interpolated onto the model time-step. The GLOMAP data (linearly interpolated to the flight track of the aircraft) and the observations are split into western and eastern regions of the Amazon (Fig. 2 and Fig. S1) and by time (Phase 1: 13/09/2012 – 22/09/2012, Phase 2: 23/09/2012 - 03/10/2012) for the western region.

References

- Allan, J. D., Morgan, W. T., Darbyshire, E., Flynn, M. J., Williams, P. I., Oram, D. E., Artaxo, P., Brito, J., Lee, J. D. and Coe, H.: Airborne observations of IEPOX-derived isoprene SOA in the Amazon during SAMBBA, *Atmos. Chem. Phys.*, 14(20), 11393–11407, doi:10.5194/acp-14-11393-2014, 2014.
- Arnott, W. P., Hamasha, K., Moosmüller, H., Sheridan, P. J. and Ogren, J. A.: Towards Aerosol Light-Absorption Measurements with a 7-Wavelength Aethalometer: Evaluation with a Photoacoustic Instrument and 3-Wavelength Nephelometer, *Aerosol Sci. Technol.*, 39(1), 17–29, doi:10.1080/027868290901972, 2005.
- Bahreini, R., Ervens, B., Middlebrook, a. M., Warneke, C., de Gouw, J. a., DeCarlo, P. F., Jimenez, J. L., Brock, C. a., Neuman, J. a., Ryerson, T. B., Stark, H., Atlas, E., Brioude, J., Fried, a., Holloway, J. S., Peischl, J., Richter, D., Walega, J., Weibring, P., Wollny, a. G. and Fehsenfeld, F. C.: Organic aerosol formation in urban and industrial plumes near Houston and Dallas, Texas, *J. Geophys. Res.*, 114, D00F16, doi:10.1029/2008JD011493, 2009.
- Baumgardner, D., Kok, G. and Raga, G.: Warming of the Arctic lower stratosphere by light absorbing particles, *Geophys. Res. Lett.*, 31(6), doi:10.1029/2003GL018883, 2004.
- Brito, J., Rizzo, L. V., Morgan, W. T., Coe, H., Johnson, B., Haywood, J., Longo, K., Freitas, S., Andreae, M. O. and Artaxo, P.: Ground-based aerosol characterization during the South American Biomass Burning Analysis (SAMBBA) field experiment, *Atmos. Chem. Phys.*, 14(22), 12069–12083, doi:10.5194/acp-14-12069-2014, 2014.
- Canagaratna, M. R., Jayne, J. T., Jimenez, J. L., Allan, J. D., Alfarra, M. R., Zhang, Q., Onasch, T. B., Drewnick, F., Coe, H., Middlebrook, A., Delia, A., Williams, L. R., Trimborn, A. M., Northway, M. J., Decarlo, P. F., Kolb, C. E., Davidovits, P. and Worsnop, D. R.: Chemical and microphysical characterization of ambient aerosols with the aerodyne aerosol mass spectrometer, *Mass Spectrom. Rev.*, 26, 185–222, doi:10.1002/mas, 2007.
- Crenn, V., Sciare, J., Croteau, P. L., Verlhac, S., Fröhlich, R., Belis, C. A., Aas, W., Äijälä, M., Alastuey, A., Artiñano, B., Baisnée, D., Bonnaire, N., Bressi, M., Canagaratna, M., Canonaco, F., Carbone, C., Cavalli, F., Coz, E., Cubison, M. J., Esser-Gietl, J. K., Green, D. C., Gros, V., Heikkinen, L., Herrmann, H., Lunder, C., Minguillón, M. C., Močnik, G., O'Dowd, C. D., Ovadnevaite, J., Petit, J. E., Petralia, E., Poulain, L., Priestman, M., Riffault, V., Ripoll, A., Sarda-Estève, R., Slowik, J. G., Setyan, A., Wiedensohler, A., Baltensperger, U., Prévôt, A. S. H., Jayne, J. T. and Favez, O.: ACTRIS ACSM intercomparison - Part 1: Reproducibility of concentration and fragment results from 13 individual Quadrupole Aerosol Chemical Speciation Monitors (Q-ACSM) and consistency with co-located instruments, *Atmos. Meas. Tech.*, 8(12), 5063–5087, doi:10.5194/amt-8-5063-2015, 2015.
- Drewnick, F., Hings, S. S., DeCarlo, P., Jayne, J. T., Gonin, M., Fuhrer, K., Weimer, S., Jimenez, J. L., Demerjian, K. L., Borrmann, S. and Worsnop, D. R.: A New Time-of-Flight Aerosol Mass Spectrometer (TOF-AMS)—Instrument Description and First Field Deployment, *Aerosol Sci. Technol.*, 39(7), 637–658, doi:10.1080/02786820500182040, 2005.
- Giles, D. M., Sinyuk, A., Sorokin, M. G., Schafer, J. S., Smirnov, A., Slutsker, I., Eck, T. F., Holben, B. N., Lewis, J. R., Campbell, J. R., Welton, E. J., Korkin, S. V., and Lyapustin, A. I.: Advancements in the Aerosol Robotic Network (AERONET) Version 3 database – automated near-real-time quality control algorithm with improved cloud screening for Sun

photometer aerosol optical depth (AOD) measurements, *Atmos. Meas. Tech.*, 12, 169-209, <https://doi.org/10.5194/amt-12-169-2019>, 2019.

- Gunthe, S. S., King, S. M., Rose, D., Chen, Q., Roldin, P., Farmer, D. K., Jimenez, J. L., Artaxo, P., Andreae, M. O., Martin, S. T., and Pöschl, U.: Cloud condensation nuclei in pristine tropical rainforest air of Amazonia: size-resolved measurements and modeling of atmospheric aerosol composition and CCN activity, *Atmos. Chem. Phys.*, 9, 7551-7575, doi:10.5194/acp-9-7551-2009, 2009.
- Heim, M., Mullins, B. J., Umhauer, H. and Kasper, G.: Performance evaluation of three optical particle counters with an efficient "multimodal" calibration method, *J. Aerosol Sci.*, 39(12), 1019–1031, doi:10.1016/j.jaerosci.2008.07.006, 2008.
- Levy, R. C., Remer, L. A., Kleidman, R. G., Mattoo, S., Ichoku, C., Kahn, R., and Eck, T. F.: Global evaluation of the Collection 5 MODIS dark-target aerosol products over land, *Atmos. Chem. Phys.*, 10, 10399-10420, <https://doi.org/10.5194/acp-10-10399-2010>, 2010.
- Mann, G. W., Carslaw, K. S., Spracklen, D. V., Ridley, D. A., Manktelow, P. T., Chipperfield, M. P., Pickering, S. J., and Johnson, C. E.: Description and evaluation of GLOMAP-mode: a modal global aerosol microphysics model for the UKCA composition-climate model, *Geosci. Model Dev.*, 3, 519-551, doi:10.5194/gmd-3-519-2010, 2010.
- McMeeking, G. R., Hamburger, T., Liu, D., Flynn, M., Morgan, W. T., Northway, M., Highwood, E. J., Krejci, R., Allan, J. D., Minikin, A. and Coe, H.: Black carbon measurements in the boundary layer over western and northern Europe, *Atmos. Chem. Phys.*, 10(19), 9393–9414, doi:10.5194/acp-10-9393-2010, 2010.
- Middlebrook, A. M., Bahreini, R., Jimenez, J. L. and Canagaratna, M. R.: Evaluation of Composition-Dependent Collection Efficiencies for the Aerodyne Aerosol Mass Spectrometer using Field Data, *Aerosol Sci. Technol.*, 46(3), 258–271, doi:10.1080/02786826.2011.620041, 2012.
- Morgan, W. T., Allan, J. D., Bower, K. N., Capes, G., Crosier, J., Williams, P. I., and Coe, H.: Vertical distribution of sub-micron aerosol chemical composition from North-Western Europe and the North-East Atlantic, *Atmos. Chem. Phys.*, 9, 5389-5401, <https://doi.org/10.5194/acp-9-5389-2009>, 2009.
- Ng, N. L., Herndon, S. C., Trimborn, A., Canagaratna, M. R., Croteau, P. L., Onasch, T. B., Sueper, D., Worsnop, D. R., Zhang, Q., Sun, Y. L. and Jayne, J. T.: An Aerosol Chemical Speciation Monitor (ACSM) for Routine Monitoring of the Composition and Mass Concentrations of Ambient Aerosol, *Aerosol Sci. Technol.*, 45(7), 780–794, doi:10.1080/02786826.2011.560211, 2011.
- Petters, M. D. and Kreidenweis, S. M.: A single parameter representation of hygroscopic growth and cloud condensation nucleus activity, *Atmos. Chem. Phys.*, 7, 1961-1971, doi:10.5194/acp-7-1961-2007, 2007.
- Reddington, C. L., Spracklen, D. V., Artaxo, P., Ridley, D. A., Rizzo, L. V., and Arana, A.: Analysis of particulate emissions from tropical biomass burning using a global aerosol model and long-term surface observations, *Atmos. Chem. Phys.*, 16, 11083-11106, <https://doi.org/10.5194/acp-16-11083-2016>, 2016.
- Schmid, O., Artaxo, P., Arnott, W. P., Chand, D., Gatti, L. V., Frank, G. P., Hoffer, A., Schnaiter, M. and Andreae, M. O.: Spectral light absorption by ambient aerosols influenced by biomass burning in the Amazon Basin. I: Comparison and field calibration of absorption

measurement techniques, *Atmos. Chem. Phys.*, 6(11), 3443–3462, doi:10.5194/acp-6-3443-2006, 2006.

Schwarz, J. P., Gao, R. S., Spackman, J. R., Watts, L. A., Thomson, D. S., Fahey, D. W., Ryerson, T. B., Peischl, J., Holloway, J. S., Trainer, M., Frost, G. J., Baynard, T., Lack, D. A., de Gouw, J. A., Warneke, C. and Del Negro, L. A.: Measurement of the mixing state, mass, and optical size of individual black carbon particles in urban and biomass burning emissions, *Geophys. Res. Lett.*, 35(13), L13810, doi:10.1029/2008GL033968, 2008.

Shiraiwa, M., Kondo, Y., Moteki, N., Takegawa, N., Sahu, L. K., Takami, A., Hatakeyama, S., Yonemura, S. and Blake, D. R.: Radiative impact of mixing state of black carbon aerosol in Asian outflow, *J. Geophys. Res.*, 113(D24), D24210, doi:10.1029/2008JD010546, 2008.

Stephens, M., Turner, N. and Sandberg, J.: Particle identification by laser-induced incandescence in a solid-state laser cavity, *Appl. Opt.*, 42(19), 3726, doi:10.1364/AO.42.003726, 2003.

Stokes, R. H. and Robinson, R. A.: Interactions in aqueous nonelectrolyte solutions. I. Solute-solvent equilibria, *J. Phys. Chem.*, 70, 2126-2130, 1966.

Trembath, J. A.: Airborne CCN Measurements, Ph.D. thesis, Faculty of Engineering and Physical Sciences, University of Manchester, UK., 2013.

van der Werf, G. R., Randerson, J. T., Giglio, L., Collatz, G. J., Mu, M., Kasibhatla, P. S., Morton, D. C., DeFries, R. S., Jin, Y., and van Leeuwen, T. T.: Global fire emissions and the contribution of deforestation, savanna, forest, agricultural, and peat fires (1997-2009), *Atmos. Chem. Phys.*, 10, 11707-11735, doi:10.5194/acp-10-11707-2010, 2010.

van der Werf, G. R., Randerson, J. T., Giglio, L., van Leeuwen, T. T., Chen, Y., Rogers, B. M., Mu, M. Q., Van Marle, M. J. E., Morton, D. C., Collatz, G. J., Yokelson, R. J., and Kasibhatla, P. S.: Global fire emissions estimates during 1997-2016, *Earth Syst. Sci. Data*, 9, 697-720, 2017.

Wang, S. C. and Flagan, R. C.: Scanning Electrical Mobility Spectrometer, *Aerosol Sci. Technol.*, 13(2), 230–240, doi:10.1080/02786829008959441, 1990.